Supplement of Biogeosciences, 20, 4477–4490, 2023
https://doi.org/10.5194/bg-20-4477-2023-supplement

Biogeosciences Open Access EGU

Supplement of

Anthropogenic climate change drives non-stationary phytoplankton internal variability

Geneviève W. Elsworth et al.

Correspondence to: Geneviève W. Elsworth (genevieve.w.elsworth@nasa.gov)

Supplemental information

In our discussion of zooplankton grazing as a contributor to changing phytoplankton internal variability with anthropogenic warming, we consider the parameterization of zooplankton grazing in the CESM1-LE. The biogeochemical ecosystem model simulates a single generic zooplankton functional type (ZFT) with different grazing rates and half saturation constants prescribed for different PFTs (e.g. slower zooplankton grazing rates for larger phytoplankton). Grazing rate for the single ZFT is computed using a Holling Type III (sigmoidal) relationship:

$$G = g_{max} \cdot T_{lim} \cdot Z \cdot \frac{P^2}{P^2 + K^2} \tag{4}$$

where g_{max} is the maximum grazing rate, T_{lim} is the temperature limitation (Q10) function, Z is the zooplankton concentration, P is the phytoplankton concentration, and K is the half-saturation constant for grazing. Zooplankton loss scales with temperature and a linear mortality term which represents zooplankton losses from predation.

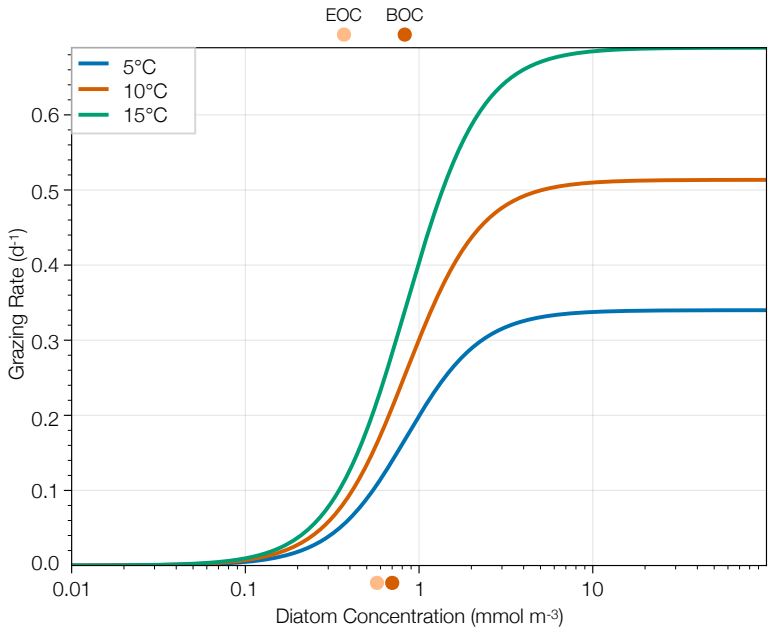

Figure S1. Holling Type III (sigmoidal) functional parameterization of zooplankton grazing rate in the biogeochemical ecosystem model of the CESM1-LE across a range of temperatures. Changes in diatom concentration between the beginning and end of the century (BOC and EOC, respectively) are shown in the dark and light orange circles, respectively, with the changes in the ASP region shown above and changes in the SAP region shown below.

Figure S1 illustrates changes in grazing rate as a function of diatom concentration using this parameterization. To approximate the effects of climatic warming, we plot the relationship for across a series of increasing temperatures: (blue) 5°C, (orange)

10°C, and (green) 15°C. The maximum grazing rate increases with warming temperatures. Changes in diatom concentration in mmol m^{-3} between the beginning and end of the century are denoted by dark and light orange circles, respectively.

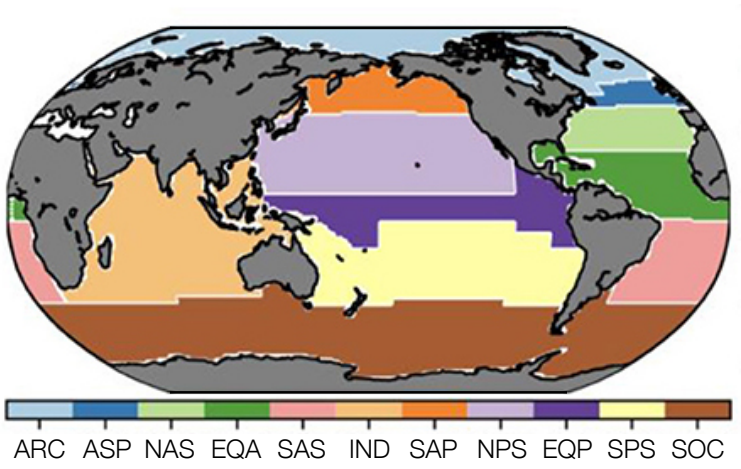

Figure S2. The 11 ocean ecological provinces defined in Tagliabue et al. (2021) and Vichi et al. (2011). Provinces were aggregated using multivariate statistical analysis of physical (i.e., salinity, temperature, mixed layer depth) and biological (i.e., chlorophyll concentration) ocean parameters to group ocean regions with similar physical and environmental conditions. Figure adapted from Tagliabue et al. (2021).

Table S1. The temporal standard deviation of phytoplankton biomass ($\sigma_{temporal}$) for ensemble member 1 of the CESM1-LE and the satellite observations from 1998 to 2019 averaged across the 11 ecological provinces defined in Vichi et al. (2011) and Tagliabue et al. (2021). Units are mg C m^{-3}.

Biome	Name	$\sigma_{temporal}, model$	$\sigma_{temporal}, obs$
ARC	Arctic	2.7	4.5
ASP	Atlantic subpolar	9.7	4.1
NAS	North Atlantic subtropical gyre	2.8	1.7
EQA	Equatorial Atlantic	1.3	1.4
SAS	South Atlantic subtropical gyre	1.1	1.2
IND	Indian Ocean	0.81	2.0
SAP	subarctic Pacific	3.7	4.0
NPS	North Pacific subtropical gyre	0.85	1.5
EQP	Equatorial Pacific	5.8	1.8
SPS	South Pacific subtropical gyre	0.60	0.93
SOC	Southern Ocean	2.7	2.7

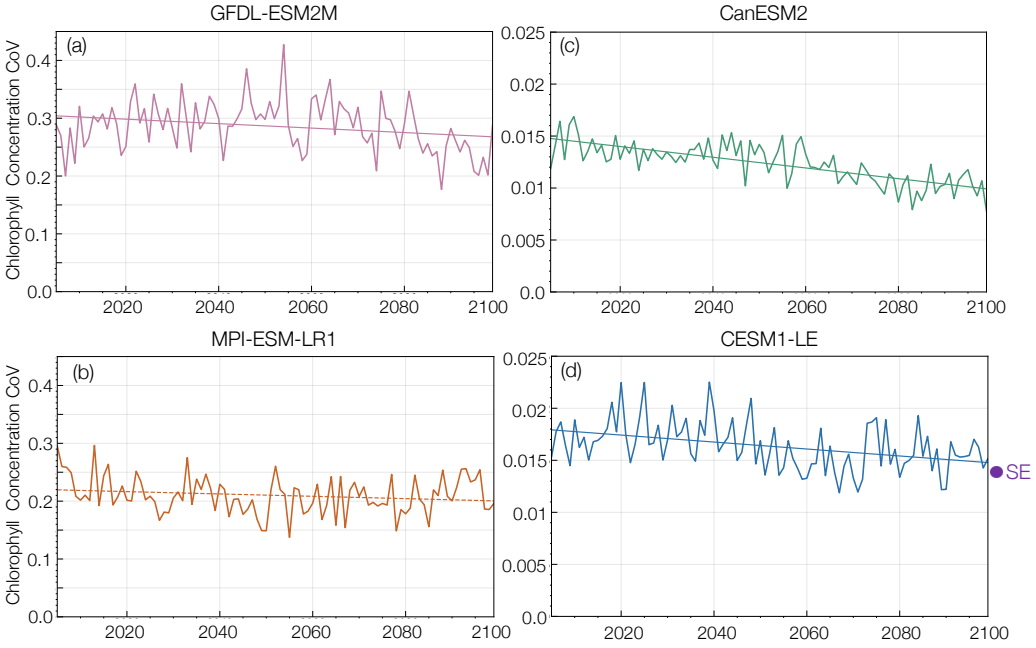

Figure S3. Coefficient of variation (internal standard deviation divided by ensemble mean) in annual mean global surface ocean chlorophyll concentration from 2006 to 2100 across a suite of CMIP5 model ensembles: (a) (pink) GFDL-ESM2M (b) (orange) MPI-ESM-LR1 (c) (green) CanESM2 (d) (blue) CESM1-LE. The average coefficient of variation of the synthetic ensemble (SE) created using the MODIS surface ocean chlorophyll record is shown in the purple dot on the vertical axis (Elsworth et al., 2020, 2021). Trend significance is determined by a t-test with a p-value less than 0.05.

To provide context for the CESM1-LE results, we examine changes in chlorophyll internal variability from a subset of the Coupled Model Intercomparison Project 5 (CMIP5) models (Taylor et al., 2011): the GFDL-ESM2M from the Geophysical Fluid Dynamics Laboratory (GFDL; (Dunne et al., 2012, 2013), the CanESM2 from the Canadian Centre for Climate Modelling and Analysis (Christian et al., 2010; Arora et al., 2011), and the MPI-ESM-LR from the Max Planck Institute (MPI; (Giorgetta et al., 2013; Ilyina et al., 2013), consisting of 30, 50, and 100 ensemble members, respectively. Similarly to the CESM1-LE, historical forcing was applied through 2005, followed by RCP8.5 forcing through 2100.

We compare the internal variability in chlorophyll observed among the large ensembles to a synthetic ensemble generated from observational chlorophyll concentrations over the MODIS remote sensing record (Elsworth et al., 2020, 2021). A synthetic ensemble is a technique that allows the observational record to be statistically emulated to create multiple possible evolutions of the observed record, each with a unique sampling of internal climate variability (McKinnon et al., 2017; McKinnon and Deser, 2018). We use the synthetic ensemble of chlorophyll concentration to compare the variability observed in the real world to the variability simulated across a suite of ESM ensembles.

Table S2. Summary statistics for the t-test performed on total phytoplankton biomass to determine trend significance across the RCP8.5 forcing scenario (2006 to 2100). Datasets are normally distributed.

Variable	Sample Size	Mean	Standard Error	95% CI
Total Phytoplankton Biomass Mean Trend	94	-0.0697	0.00459	-0.0743 to -0.0651
Total Phytoplankton Biomass Standard Deviation Trend	94	-0.0164	0.00323	-0.0196 to -0.0132

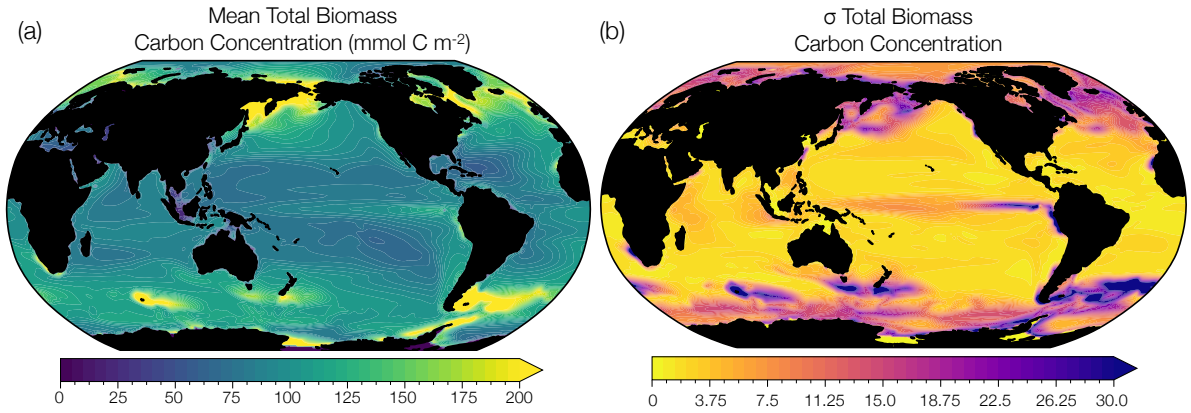

Figure S4. (a) Total phytoplankton carbon concentration simulated by the CESM1-LE in mmol C m^{-2} averaged across the RCP8.5 forcing scenario (2006 to 2100). (b) Internal standard deviation in total phytoplankton carbon concentration averaged over the same period. The change in the coefficient of variation is calculated using averages across the first (2006 to 2016) and last (2090 to 2100) decades of the RCP8.5 forcing scenario.

585 To provide context for Figure 3, we include the spatial distribution of total phytoplankton carbon concentration (Figure S4a) and internal standard deviation in phytoplankton carbon concentration (Figure S4b) simulated by the CESM1-LE across the RCP8.5 forcing scenario (2006 to 2100). Total phytoplankton carbon concentration is relatively high in the subpolar Atlantic and Pacific, the Southern Ocean, and the Eastern Equatorial Upwelling Zone and relatively low in the subtropical gyre regions (Figure S4a). Regions of relatively high phytoplankton carbon concentrations correspond to regions of high internal variability
590 (Figure S4b).